RESEARCH ARTICLE

Photocatalytic degradation of methylene blue by zinc oxide/iron oxide/copper oxide nanocomposites under visible light

Zaizhen Zhang[†], Zhenyan Yin[*], Cui Jiang[†]

Agriculture and Forestry Technology School, Weifang Engineering Vocational College, Qingzhou, Shandong, China.

Received: April 13, 2026; **accepted:** July 28, 2026.

Methylene blue is widely generated from textiles, dyeing, and papermaking wastewater, and its discharge can cause water coloration and damage aquatic ecosystems. Existing methods such as adsorption, coagulation, and biological treatment often suffer from pollutant transfer, secondary waste generation, or incomplete degradation. Visible-light photocatalysis can utilize solar energy to promote the deep oxidation of dyes, therefore, developing highly efficient visible-light-responsive photocatalytic materials is of great significance. A ternary nanocomposite material of zinc oxide/ferric oxide/copper oxide was prepared in this study using a sol-gel-hydrothermal combined process. The material's structure and properties were clarified, and its photocatalytic degradation performance of methylene blue was investigated. The results showed that the tightly bound type-II heterojunction formed by zinc oxide, ferric oxide, and copper oxide in the composite material effectively promoted the spatial separation and interfacial transport of photogenerated carriers. The light absorption range of the composite material extended to the entire visible light region, and the band gap was adjusted to 2.15 eV. Under visible-light irradiation, the degradation rate of methylene blue by zinc oxide/ferric oxide/copper oxide reached 96.8%, which was superior to that of any single component. The degradation process was dominated by photogenerated holes (H^+) and hydroxyl radicals (·OH), and the strong adsorption of methylene blue on the material surface further promoted the interfacial reaction. Furthermore, the composite material exhibited excellent cycling stability with 90.2% activity retention after 5 cycles and superparamagnetic with saturation magnetization of 18.6 emu/g, enabling convenient magnetic separation and recovery of the catalyst. This research provided technical support for the development of efficient, stable, and easily recoverable multi-component photocatalysts.

Keywords: methylene blue; photocatalytic degradation; ternary nanocomposite materials; magnetic separation; cycle stability; catalyst; water pollution.

[*]**Corresponding author:** Zhenyan Yin, Agriculture and Forestry Technology School, Weifang Engineering Vocational College, Qingzhou, Shandong 262500, China. Email: yinzhenyan513@163.com.

[†]These authors contributed equally to this work.

Introduction

With the rapid development of textiles, dyeing, papermaking, and chemical industries, the discharge of dye-containing wastewater has continued to increase. Such wastewater is generally characterized by complex composition, high chromaticity, strong toxicity, and poor biodegradability, and has therefore become an important challenge in aquatic environmental remediation [1]. Methylene blue (MB) is a typical phenothiazine cationic dye that is widely used in

the textile, printing, and papermaking industries. When MB-containing wastewater is discharged into aquatic environments without adequate treatment, it can not only cause water coloration and reduce light penetration but also inhibit photosynthesis in aquatic plants and potentially threaten ecosystems and human health through bioaccumulation and food-chain transfer [2]. At present, the main treatment methods for MB-containing wastewater include adsorption, coagulation-precipitation, membrane separation, and biological treatment. However, these methods still suffer from several limitations such as pollutant transfer, secondary waste generation, high operating costs, or incomplete degradation. In contrast, photocatalytic technology has the advantages of mild reaction conditions, limited secondary pollution, and high mineralization efficiency, and is therefore regarded as an important approach for treating dyed wastewater. Its effectiveness largely depends on the development of efficient and stable photocatalytic materials with strong visible-light responsiveness [3].

Zinc oxide (ZnO) is a typical n-type semiconductor photocatalyst with strong redox ability, good chemical stability, environmental friendliness, and low cost, and has been widely investigated for the photocatalytic degradation (PD) of organic pollutants [4]. However, ZnO has a band gap of approximately 3.2 eV and responds mainly to ultraviolet light, which accounts for only a small fraction of the solar spectrum. Consequently, its solar-energy utilization efficiency is relatively low. In addition, photogenerated electron-hole pairs in ZnO recombine rapidly, which restricts further improvement in its photocatalytic performance [5]. Iron oxide (Fe_3O_4) is a semiconductor material with magnetic responsiveness and a band gap of approximately 1.98 eV. It can respond to part of the visible-light spectrum and can be rapidly separated and recovered under an external magnetic field because of its superparamagnetic properties, thereby reducing catalyst loss and the risk of secondary pollution [6]. However, single-phase Fe_3O_4 exhibits low photogenerated-carrier separation efficiency and limited photocatalytic activity, making it difficult to satisfy the requirements of highly efficient degradation when used alone [7]. Copper oxide (CuO) is a p-type semiconductor with a band gap of approximately 1.85 eV, strong visible-light absorption, and favorable electron-transport properties. It is therefore commonly combined with other semiconductors to construct heterojunctions and improve photocatalytic performance [8]. Nevertheless, pure CuO has a relatively small specific surface area and a high probability of photogenerated-carrier recombination, and its photocatalytic efficiency remains limited when used independently [9]. To overcome the limitations of individual metal oxides in terms of light-absorption range and carrier separation, the construction of multicomponent heterojunction systems has become an important strategy for photocatalyst modification. Through rational matching of the band structures of different semiconductors, effective charge-transfer channels can be formed at the interfaces, thereby promoting the spatial separation of photogenerated electrons and holes and reducing their recombination probability. In addition, multicomponent composites can integrate the functional advantages of different materials such as the strong oxidation ability of ZnO, the magnetic-separation capability of Fe_3O_4, and the visible-light responsiveness of CuO, thereby generating synergistic effects [10]. In recent years, considerable progress has been made in this field. Liu *et al.* prepared a ZnO/Fe_3O^4 magnetic composite photocatalyst using a coprecipitation–hydrothermal method. The results showed that the composite exhibited significantly higher MB degradation activity under visible-light irradiation than pure ZnO and could be rapidly separated and recovered using an external magnetic field [11]. Abdul-Ameer *et al*. constructed a ZnO/CuO p-n heterojunction through a solvothermal method. The study demonstrated that band-structure matching in the heterojunction facilitated interfacial charge transfer, effectively suppressed the recombination of photogenerated electron-hole

pairs, and thereby improved photocatalytic performance [12]. These findings indicate that binary heterojunctions can improve the visible-light response and carrier-separation efficiency of individual semiconductor materials to a certain extent. Compared with binary composites, ternary heterojunction systems can further regulate band structures and charge-transfer pathways through the synergistic interaction of three semiconductors, while simultaneously improving photocatalytic activity, stability, and recyclability. The ZnO/Fe_3O_4/CuO ternary composite system combines the strong oxidation ability of ZnO, the magnetic-separation characteristics of Fe_3O_4, and the broad visible-light response of CuO, and is therefore expected to exhibit superior photocatalytic performance. However, research on this ternary system remains relatively limited, and several issues still require urgent attention, which include that existing preparation methods can easily result in uneven component dispersion, particle agglomeration, and insufficient heterojunction interfacial contact, which adversely affect the interfacial transport efficiency of photogenerated carriers. The structure-activity relationship between the microscopic structure of the three components and their photocatalytic performance has not yet been fully clarified. No unified understanding has been reached regarding the charge-transfer pathways, dominant reactive species, and their respective contributions to the degradation reaction in this ternary system [13]. In addition, the cycling stability and magnetic-separation performance of the composite materials still need to be further improved to meet the practical requirements of efficient, stable, and reusable catalysts for dye-wastewater treatment.

This study proposed a ZnO/Fe_3O_4/CuO ternary nanocomposite using a combined sol-gel-hydrothermal method. The sol-gel process enabled homogeneous mixing of different metal precursors at the molecular or ionic level, while the subsequent hydrothermal treatment promoted crystal growth and heterointerface formation, thereby improving component dispersion and interfacial bonding. The structural characteristics and band-gap changes of the composite were investigated through analyses of crystal structure, elemental composition, surface chemical states, and optical properties. Its photocatalytic performance toward MB under visible-light irradiation was evaluated through degradation experiments. Free-radical-trapping experiments were conducted to identify the dominant reactive species and clarify the photocatalytic mechanism, while cycling tests and magnetic measurements were performed to assess its stability and recoverability. This study revealed the synergistic interactions and structure-activity relationships among ZnO, Fe_3O_4, and CuO, thereby providing a theoretical basis and technical support for the design of efficient, stable, and easily recoverable visible-light-responsive photocatalysts, as well as a reference for the advanced treatment of dye wastewater and the engineering application of multicomponent photocatalytic materials.

Materials and methods

Preparation of ZnO/Fe_3O4/CuO nanocomposite

A ZnO/Fe_3O_4/CuO ternary nanocomposite was prepared using a combined sol–gel–hydrothermal method. Zinc nitrate hexahydrate ($Zn(NO_3)_2{\cdot}6H_2O$), iron nitrate nonahydrate ($Fe(NO_3)_3{\cdot}9H_2O$), copper sulfate pentahydrate ($CuSO_4{\cdot}5H_2O$) (Shanghai Macklin Biochemical Co., Ltd., Shanghai, China) were weighed according to a Zn:Fe:Cu molar ratio of 3:1:1 and added to 50 mL of a mixed solvent containing ethylene glycol and deionized water at a volume ratio of 1:1. Subsequently, 0.5 g of cetyltrimethylammonium bromide (CTAB) (Shanghai Aladdin Biochemical Technology Co., Ltd., Shanghai, China) was added as a dispersant, and the mixture was stirred at 60°C for 30 min using an HW-S2 thermostatic magnetic stirrer (Hangzhou Qiwei Instrument Co., Ltd., Hangzhou, Zhejiang, China) until the three metal salts were completely dissolved and a homogeneous transparent mixed-salt solution was obtained. In this system, Zn^{2+}, Fe^{3+}, and Cu^{2+} were uniformly dispersed at a molar ratio of

3:1:1, while CTAB inhibited the aggregation of metal ions and subsequently formed particles through surface adsorption and steric hindrance. Under continuous stirring, 1 mol/L NaOH solution was slowly added dropwise to the mixed-salt solution until the pH reached 9.0. The mixture was then stirred for an additional 60 min to form a stable sol before transferring into a KH-100 100 mL Teflon-lined hydrothermal reactor (Xi'an Taikang Biotechnology Co., Ltd., Xi'an, Shaanxi, China), sealed, and placed in a DZF-6050 constant-temperature drying oven (Shanghai Yiheng Scientific Instrument Co., Ltd., Shanghai, China) at 160°C for 8 h. After the hydrothermal reaction, the reactor was naturally cooled to room temperature. The product was centrifuged at 8,000 rpm for 10 min using a TG16-WS high-speed centrifuge (Hunan Xiangyi Laboratory Instrument Development Co., Ltd., Changsha, Hunan, China). The precipitate was collected and alternately washed five times with deionized water and absolute ethanol to remove residual electrolytes, unreacted precursors, and organic impurities. The washed precipitate was dried at 60°C for 12 h to obtain loose precursor powder. The precursor mainly consisted of low-crystallinity metal hydroxides or oxyhydroxides and possibly contained intermediate phases such as $Zn(OH)_2$, FeOOH, and $Cu(OH)_2$. During coprecipitation, the different metal components formed closely contacted Zn–O–Fe and Fe–O–Cu interfaces. CTAB promoted the formation of a relatively loose porous structure and reduced particle agglomeration. These structural characteristics provided a basis for the subsequent formation of ZnO, Fe_3O_4, and CuO phases and heterointerfaces during calcination. The dried precursor powder was placed in an alumina crucible and heated in a BYT-600 tube furnace (Nanjing Boyuntong Instrument Technology Co., Ltd., Nanjing, Jiangsu, China) from room temperature to 500°C at a heating rate of 5°C/min and maintained at this temperature for 2 h. After calcination, the sample was naturally cooled to room temperature in the furnace and ground to obtain the $ZnO/Fe_3O_4/CuO$ ternary nanocomposite. Pure ZnO, Fe_3O_4, and CuO reference samples were prepared under the same synthesis and heat-treatment conditions, except that only the corresponding single-metal precursor was used.

X-ray diffraction analysis

The crystal structures and phase compositions of ZnO, Fe_3O_4, CuO, and $ZnO/Fe_3O_4/CuO$ were analyzed using a SmartLab X-ray diffractometer (Rigaku Corporation, Tokyo, Japan). Before measurement, the dried powder was uniformly loaded into a sample holder and leveled. Cu Kα radiation with a wavelength of 1.5406 Å was used as the radiation source. The tube voltage and current were set to 40 kV and 40 mA, respectively. The diffraction patterns were recorded over a 2θ range of 10° - 80° at a scanning rate of 5°/min and a step size of 0.02°. The crystalline phases were identified by comparison with standard diffraction cards, and the average crystallite sizes corresponding to the major diffraction peaks were estimated using the Scherrer method.

Raman spectroscopy analysis

The lattice vibrations and chemical bonding characteristics of the materials were analyzed using inVia Reflex Raman spectrometer (Renishaw plc, Wotton-under-Edge, Gloucestershire, UK). Before measurement, the powder sample was uniformly pressed onto a clean glass slide. A 532 nm laser was used as the excitation source at a laser power of 5 mW. Raman spectra were collected over the range of 100 – 1,000/cm with a spectral resolution of 1/cm and an integration time of 10 s. The characteristic peak positions, intensities, and widths were compared to identify the ZnO, Fe_3O_4, and CuO phases and evaluate lattice changes induced by the composite interfaces.

X-ray photoelectron spectroscopy analysis

The surface elemental composition and chemical valence states of the composite were analyzed using an ESCALAB 250Xi X-ray photoelectron spectrometer (Thermo Fisher Scientific, Waltham, Massachusetts, USA). The powder sample was uniformly mounted on conductive adhesive tape and placed in an ultrahigh-vacuum

chamber. Monochromatic Al Kα radiation with a photon energy of 1486.6 eV was used as the excitation source. A survey spectrum was first collected to determine the presence of Zn, Fe, Cu, and O followed by high-resolution spectra of Zn 2p, Fe 2p, Cu 2p, and O 1s. The pass energies for the survey and high-resolution spectra were set to 100 and 20 eV, respectively. All binding energies were calibrated against the C 1s peak at 284.8 eV. Background subtraction and peak fitting were performed using Avantage 5.992 software [14].

Ultraviolet-visible diffuse reflectance spectroscopy measurement

Ultraviolet–visible diffuse reflectance spectra were measured using a Lambda 950 UV–Vis–NIR spectrophotometer (PerkinElmer Inc., Waltham, Massachusetts, USA) equipped with an integrating sphere. The powder samples were uniformly packed into the sample holder, and a $BaSO_4$ standard white plate was used as the 100% reflectance reference. The spectra were recorded over the wavelength range of 200 – 800 nm at an interval of 1 nm. The diffuse reflectance data were converted into an absorption function using the Kubelka–Munk method, and the optical band gaps of ZnO, Fe_3O_4, CuO, and the composite were determined using the Tauc relation.

Elemental composition analysis

The elemental composition of the samples was determined using an X-MaxN 80 energy-dispersive X-ray spectrometer (Oxford Instruments, Abingdon, Oxfordshire, UK). The powder samples were uniformly mounted on conductive adhesive tape, and spectra were collected from multiple randomly selected regions to determine the atomic and mass percentages of Zn, Fe, Cu, and O. The elemental contents were calculated as the averages of the measurements from different regions to reduce the influence of local compositional heterogeneity.

Magnetic property analysis

The magnetic properties of the composite were measured at room temperature using a Lake Shore 7404 vibrating sample magnetometer (Lake Shore Cryotronics, Westerville, Ohio, USA). The applied magnetic field ranged from -20,000 to 20,000 Oe. The saturation magnetization, remanent magnetization, and coercivity were obtained from the magnetization-field curves and used to evaluate the magnetic separation and recovery performance of the material.

Photoelectrochemical performance analysis

Photoelectrochemical measurements were conducted using a CHI660E electrochemical workstation (Shanghai Chenhua Instrument Co., Ltd., Shanghai, China). Catalyst-coated conductive glass was used as the working electrode, a platinum sheet as the counter electrode, and an Ag/AgCl electrode as the reference electrode. A 0.5 mol/L Na_2SO_4 solution was used as the electrolyte. Transient photocurrent responses were recorded under intermittent visible-light irradiation. Electrochemical impedance spectroscopy was performed over a frequency range of 0.01 Hz to 100 kHz with an AC amplitude of 5 mV to evaluate photogenerated-carrier separation and interfacial charge-transfer performance.

Methylene blue adsorption and photocatalytic degradation experiments

Methylene blue (MB) (Shanghai Macklin Biochemical Co., Ltd., Shanghai, China) was used as the target pollutant. An MB aqueous solution with an initial concentration of 10 mg/L was prepared. A 50 mL aliquot was placed in a 100 mL beaker, and 50 mg of catalyst was added. ZnO, Fe_3O_4, CuO, and ZnO/Fe_3O_4/CuO were separately tested to compare their MB adsorption and degradation performances [15].

(1) Dark adsorption experiment

The beaker containing the MB solution and catalyst was placed on an HW-S2 thermostatic magnetic stirrer and stirred in the dark at 25 ± 1°C and 500 rpm for 30 min to establish adsorption-desorption equilibrium between MB and the catalyst surface. After dark adsorption, 5 mL of the suspension was collected and centrifuged at 8,000 rpm for 10 min. The absorbance of the

supernatant was measured at 664 nm using a 722S visible spectrophotometer (Shanghai Precision and Scientific Instrument Co., Ltd., Shanghai, China). The dark adsorption efficiency of MB was determined from the change between the initial absorbance before catalyst addition and the absorbance after adsorption equilibrium. Because the absorbance of MB at 664 nm was proportional to its concentration within the measured range according to the Beer-Lambert law, the absorbance change was used to represent the relative decrease in MB concentration.

(2) Visible-light photocatalytic degradation experiment

After adsorption-desorption equilibrium was reached, visible-light irradiation was provided using a CEL-HXF300 xenon lamp system (Beijing China Education Au-Light Co., Ltd., Beijing, China) with a power of 300 W. A 420 nm cutoff filter was used to remove ultraviolet radiation. The distance between the light source and the liquid surface was fixed at 15 cm, and the light intensity at the liquid surface was 100 mW/cm^2. During irradiation, the suspension was continuously stirred at 500 rpm to maintain uniform catalyst dispersion, and the reaction temperature was maintained at 25 ± 1°C. The suspension was irradiated for 120 min, and 5 mL aliquots were collected at 20 min intervals. Each sample was centrifuged at 8,000 rpm for 10 min to remove catalyst particles, and the absorbance of the supernatant was measured at 664 nm. No solution was added after sampling, and the cumulative loss of solution volume was corrected during data processing. The photocatalytic degradation efficiency of MB was determined from the change between the absorbance after dark adsorption equilibrium and the absorbance measured at different irradiation times. According to the Beer-Lambert law, the absorbance change was used to represent the relative change in MB concentration. The photocatalytic degradation kinetics were fitted using a pseudo-first-order kinetic model, and the apparent reaction-rate constant was obtained from the relationship between the absorbance after dark adsorption equilibrium and that at each irradiation time. All dark adsorption and photocatalytic degradation experiments were independently repeated three times [16].

Cycling stability and magnetic separation experiments

The cycling stability experiments were performed using the same MB concentration, solution volume, catalyst dosage, dark adsorption time, and irradiation conditions as those used in the initial photocatalytic degradation experiment. After each cycle, the ZnO/Fe_3O_4/CuO composite was first separated using an external magnet and then recovered by centrifugation at 8,000 rpm for 10 min. The recovered catalyst was washed three times each with deionized water and absolute ethanol to remove adsorbed MB and degradation intermediates and was then dried at 60°C for 8 h. The dried catalyst was directly reused in the next cycle. In each cycle, 50 mL of fresh MB solution at 10 mg/L was added, while all other reaction conditions remained unchanged. Five consecutive cycles were performed. No fresh catalyst was added during the cycling experiments, and the recovered catalyst mass was recorded after each cycle. The activity retention after each cycle was determined by comparing the MB degradation efficiency of that cycle with that of the first cycle. This value was used to evaluate the retention of photocatalytic activity during repeated use. After five cycles, the recovered catalyst was reanalyzed by XRD to compare its crystal structure before and after cycling.

Reactive species trapping experiment

To identify the major reactive species involved in photocatalytic degradation, specific scavengers were separately added to the reaction system. A 50 mg portion of the ZnO/Fe_3O_4/CuO composite was added to 50 mL of a 10 mg/L MB solution. Isopropanol (IPA), disodium ethylenediaminetetraacetate (EDTA-2Na), and benzoquinone (BQ) (Shanghai Macklin Biochemical Co., Ltd., Shanghai, China) were separately added to final concentrations of 1 mmol/L. IPA was used as a ·OH scavenger, EDTA-

2Na as an H^+ scavenger, and BQ as a $\cdot O^{2-}$ scavenger. A reaction system without any scavenger was used as the blank control. Each reaction system was first stirred in the dark at 500 rpm for 30 min to establish adsorption-desorption equilibrium and was then irradiated under the same visible-light conditions as those used in the photocatalytic degradation experiment for 120 min. After the reaction, 5 mL of the suspension was collected and centrifuged at 8000 rpm for 10 min. The absorbance of the supernatant was measured at 664 nm. The relative contributions of ·OH, H^+, and $\cdot O^{2-}$ to the photocatalytic degradation process were evaluated by comparing the MB degradation efficiencies of the scavenger-treated groups with that of the blank control.

Statistical analysis

All adsorption, photocatalytic degradation, reactive-species trapping, and cycling-stability experiments were independently repeated three times, and the results were expressed as mean ± standard deviation. Statistical analyses were performed using SPSS Statistics 27.0 (IBM Corp., Armonk, New York, USA). One-way analysis of variance was used to compare the dark adsorption efficiencies, 120 min degradation efficiencies, and apparent reaction-rate constants among ZnO, Fe_3O_4, CuO, and ZnO/Fe_3O_4/CuO. When the overall difference was statistically significant, Tukey's post hoc test was used for pairwise comparisons. Differences in degradation efficiency among the reactive-species scavenger groups were also analyzed using one-way analysis of variance followed by Tukey's post hoc test. Repeated measures analysis of variance was used to evaluate differences among successive cycling tests. All tests were two-sided, and $P < 0.05$ was considered statistically significant [17].

Results and discussion

Crystal structure analysis

The XRD patterns of the ZnO/Fe_3O_4/CuO nanocomposite and the single components (ZnO, Fe_3O_4, CuO) showed that the XRD pattern of the ZnO/Fe_3O_4/CuO nanocomposite exhibited obvious multi-phase superposition characteristics with no new impurity phase diffraction peaks appearing, which confirmed that the three metal oxides only underwent physical mixing and interfacial bonding during the composite process, without chemical reactions to generate impurity phases, and the crystallinity was good. Among them, the (101) plane of ZnO, the (311) plane of Fe_3O_4, and the (111) plane of CuO were the strongest peaks of their respective phases. Compared with the single components, the intensity of the diffraction peaks of each phase was slightly weakened after composite (Figure 1a). Pure ZnO had a high-purity hexagonal wurtzite structure with sharp diffraction peaks on the (101) plane, and its average grain size was calculated to be approximately 32 nm (Figure 1b). Pure Fe_3O_4 had a cubic spinel structure with obvious characteristic peaks (CPs) and a grain size of approximately 25 nm (Figure 1c). Pure CuO was a monoclinic phase with good crystallinity and a grain size of approximately 28 nm (Figure 1d). A comprehensive comparison revealed that the ZnO/Fe_3O_4/CuO nanocomposite material was beneficial for increasing the specific surface area of the composite material, furnishing more active sites for photocatalytic reactions. Simultaneously, the formation of the multi-component heterojunction enabled synergistic effects among the components, laying the structural foundation for the efficient separation and transfer of PCs and promoting photocatalytic performance. The Raman spectra of the ZnO/Fe_3O_4/CuO nanocomposite and the single components (ZnO, Fe_3O_4, CuO) demonstrated that the ZnO spectrum exhibited the strongest E2 (high) mode peak at 437/cm, along with CPs at 332, 381, and 583/cm, confirming its regular hexagonal wurtzite structure and good crystallinity (Figure 2a). The Fe_3O_4 spectrum displayed a sharp A1g CP (Fe-O bond symmetric stretching vibration) at 668/cm with other CPs at 218, 304, and 538/cm, indicating its intact cubic spinel structure (Figure 2b). The spectrum of CuO exhibited a series of CPs at 298, 344, 390, 468,

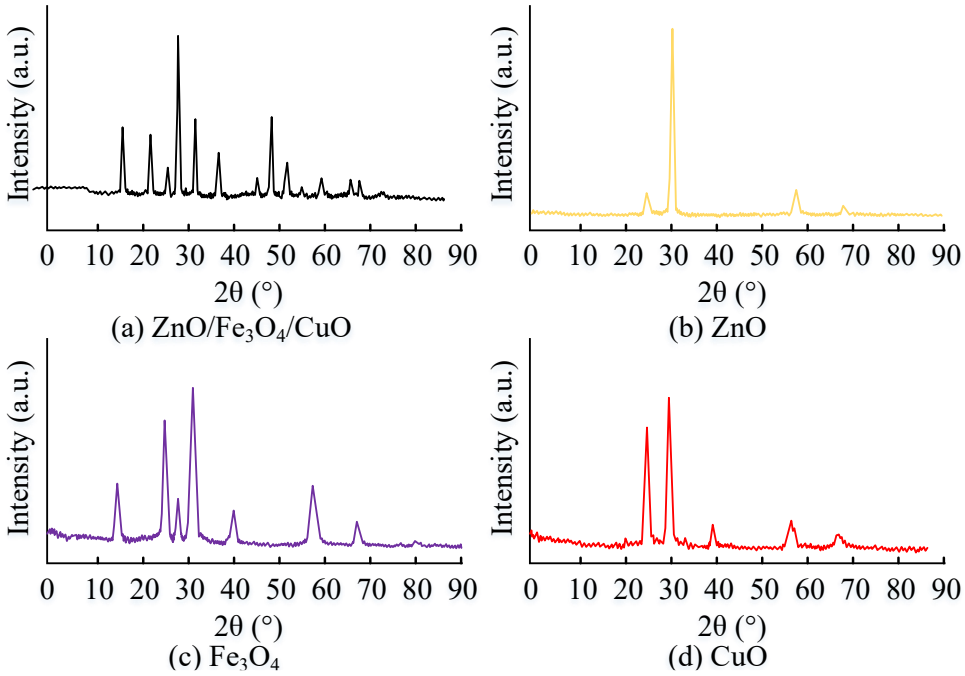

Figure 1. XRD patterns of ZnO/Fe_3O_4/CuO nanocomposites and single components nanocomposites.

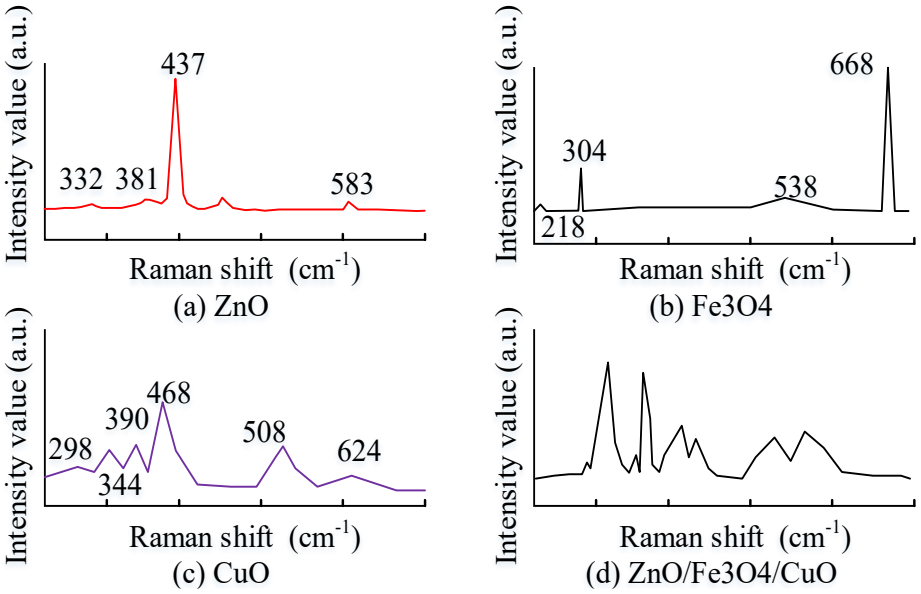

Figure 2. XRD Raman spectra of ZnO/Fe_3O_4/CuO nanocomposites and single-component nanocomposites.

508, and 624/cm, corresponding to its monoclinic phase structure with the strong peaks at 344/cm and 624/cm being particularly prominent (Figure 2c). The Raman spectrum of the composite material clearly included all the CPs of the three components ZnO, Fe_3O_4, and CuO simultaneously, without any new peaks appearing (Figure 2d), which proved that the composite process did not trigger a chemical reaction to generate a new phase, achieving physical composite and interfacial bonding of the three phases. Compared with the single

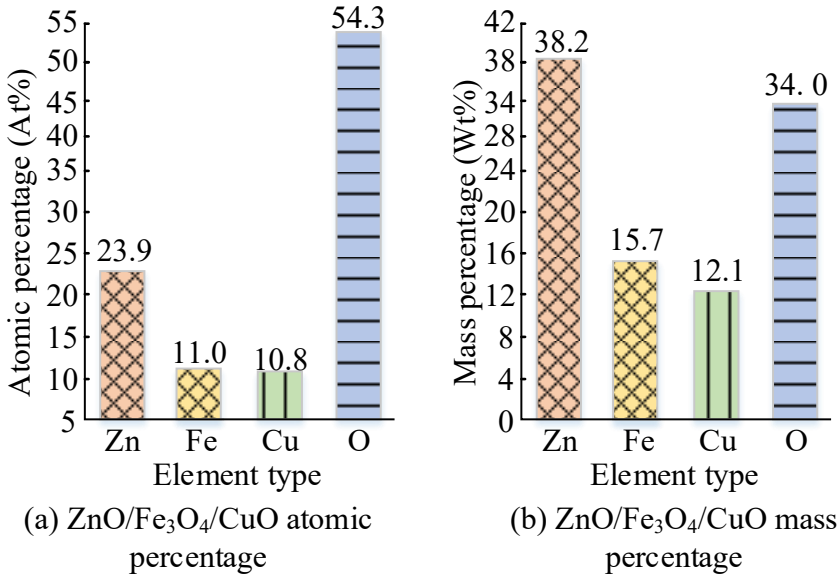

(a) $ZnO/Fe_3O_4/CuO$ atomic percentage

(b) $ZnO/Fe_3O_4/CuO$ mass percentage

Figure 3. Elemental composition of $ZnO/Fe_3O_4/CuO$ nanocomposites.

components, the intensity of each CP in the composite material was generally weakened, and some peak shapes were slightly broadened. This was attributed to the lattice distortion and interfacial stress caused by the formation of the multi-component heterojunction interface. This tight interfacial bonding was beneficial to the migration and separation of PCs between heterojunctions, thus providing a key structural basis for improving the photocatalytic performance of the composite material.

Elemental composition analysis

The elemental composition of the $ZnO/Fe_3O_4/CuO$ nanocomposite material showed that O had the highest proportion in the composite material, reaching 54.3%, which was closely linked to the lattice oxygen contributed by the three metal oxides and the adsorbed oxygen species that might exist on the surface. The atomic percentage of Zn was 23.9%, corresponding to the ZnO component, while the atomic percentages of Fe and Cu were 10.8% and 11.0%, respectively, originating from the Fe_3O_4 and CuO phases (Figure 3a). This elemental composition ratio was basically consistent with the designed feed ratio during the preparation process, and no abnormal enrichment or severe loss of any element was observed, providing a key chemical composition basis for further constructing a uniform and stable multi-element heterostructure. The mass percentages of Zn, Fe, Cu, and O were 38.2%, 15.7%, 12.1%, and 34.0%, respectively, which were basically consistent with the feed ratio during preparation, further confirming that the three components ZnO, Fe_3O_4, and CuO successfully combined to form a uniform nanocomposite material (Figure 3b).

Analysis of chemical valence state and surface electronic structure

The high-resolution XPS spectra of Zn2p, Fe2p, Cu2p, and O1s of the $ZnO/Fe_3O_4/CuO$ nanocomposite material showed that two CPs appeared in the Zn2p spectrum, located at 1,021.8 eV (Zn2p3/2) and 1,044.9 eV (Zn2p1/2) with a peak spacing of 23.1 eV, corresponding to the characteristic binding energy of Zn^{2+}, indicating that Zn existed in the composite material in the form of ZnO (Figure 4a). In the Fe2p spectrum, the CPs at 710.8 eV (Fe2p3/2) and 724.5 eV (Fe2p1/2) corresponded to Fe^{3+}, while the satellite peak at 718.5 eV and the shoulder peak near 709.5 eV confirmed the presence of Fe^{2+}, indicating that Fe existed in the form of Fe_3O_4 (Figure 4b). The CPs of Cu2p3/2 and

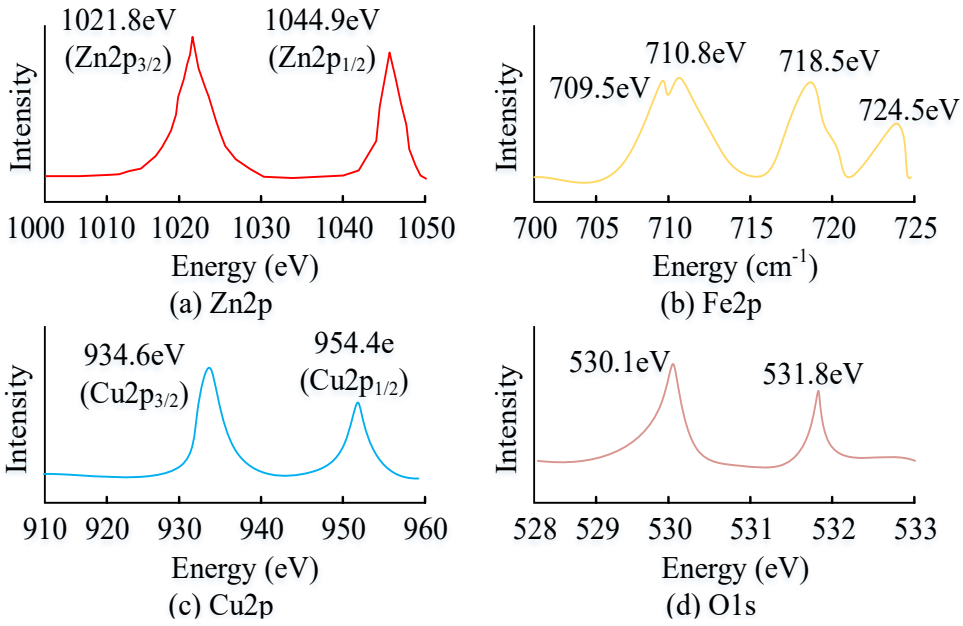

Figure 4. High-resolution XPS spectra of Zn2p, Fe2p, Cu2p, and O1s of the ZnO/Fe_3O_4/CuO nanocomposite material.

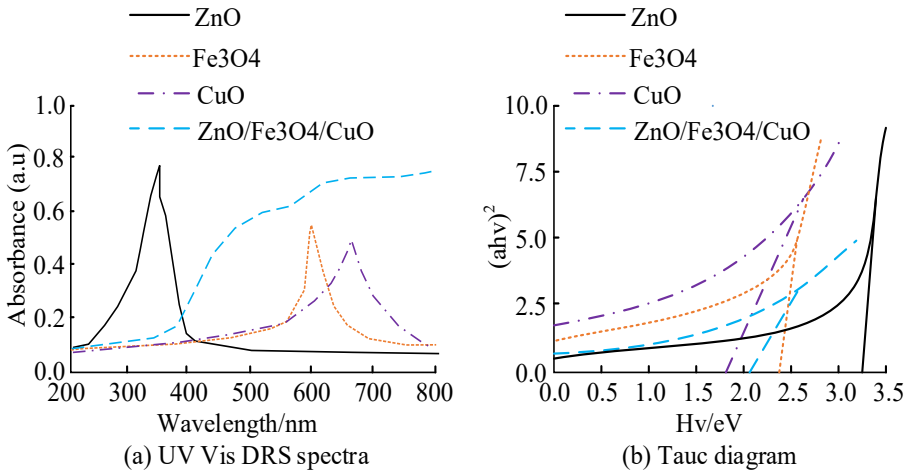

Figure 5. UV-vis DRS and Tauc plots of ZnO/Fe_3O_4/CuO nanocomposites and single components.

Cu2p1/2were located at 934.6 eV and 954.4 eV with obvious satellite peaks at 942.5 eV and 962.3 eV. These were typical characteristics of Cu^{2+}, indicating that Cu existed in the form of CuO (Figure 4c). The O1s spectrum could be divided into two peaks at 530.1 eV corresponded to lattice oxygen (MO, M = Zn, Fe, Cu) in the metal oxide and at 531.8 eV corresponded to surface adsorbed oxygen (such as -OH, adsorbed O_2). The presence of surface adsorbed oxygen was conducive to the formation of reactive oxygen species (· O^{2-}, · OH), which promoted the PD reaction (Figure 4d).

Optical performance analysis

The UV-vis DRS and Tauc spectra of the ZnO/Fe_3O_4/CuO nanocomposite and the single component showed that the light absorption of pure ZnO was mainly concentrated in the ultraviolet region with an absorption edge of

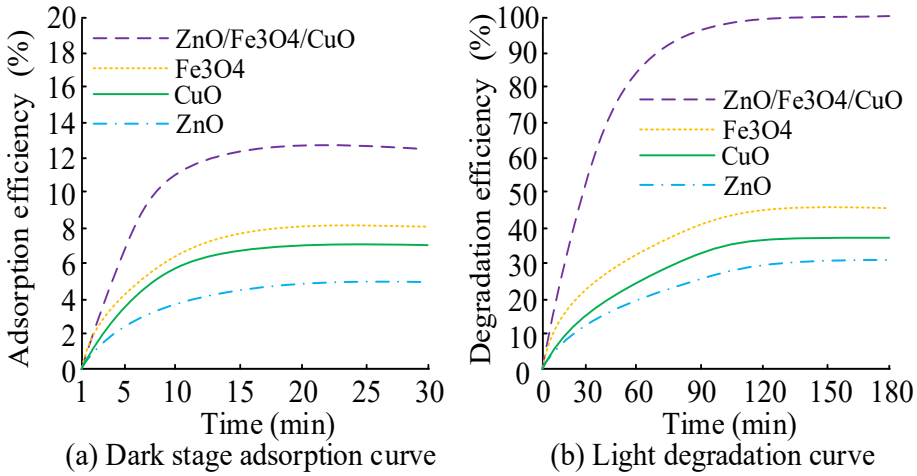

Figure 6. Adsorption and degradation results of MB by ZnO/Fe_3O_4/CuO nanocomposites and single-component adsorption.

approximately 380 nm, and it showed almost no response to VL. The absorption edges of Fe_3O_4 and CuO were located at 620 nm and 670 nm. Although they could respond to some VL, the absorption intensity was limited. In contrast, the light absorption range of the ZnO/Fe_3O_4/CuO composite significantly extended into the VL region of 400 - 800 nm, and it exhibited strong absorption intensity throughout the entire VL region (Figure 5a). The BGs of ZnO, Fe_3O_4, and CuO were 3.23 eV, 1.98 eV, and 1.85 eV. However, the BG of the ZnO/Fe_3O_4/CuO composite material was reduced to 2.15 eV, which was lower than that of ZnO but higher than that of Fe_3O_4 and CuO. This moderate BG allowed it to effectively absorb VL while ensuring that the PCs had sufficient redox capabilities (Figure 5b).

PD performance analysis

The comparison of MB adsorption and photocatalytic degradation performances of ZnO, Fe_3O_4, CuO, and ZnO/Fe_3O_4/CuO showed that, after 30 min of dark adsorption, the adsorption efficiency of the ZnO/Fe_3O_4/CuO nanocomposite was 12.5 ± 0.4%, significantly higher than those of ZnO (4.2 ± 0.2%), Fe_3O_4 (7.8 ± 0.3%), and CuO (6.5 ± 0.3%) ($F = 386.63$, $P < 0.001$). This improvement was related to the increased number of accessible adsorption sites and stronger interfacial interactions in the composite. After 120 min of visible-light irradiation, the MB degradation efficiency of the composite reached 96.8 ± 0.6%, whereas those of ZnO, Fe_3O_4, and CuO were 28.3 ± 0.4%, 42.5 ± 0.5%, and 35.7 ± 0.4%, respectively. The differences were statistically significant ($F = 12,555.47$, $P < 0.001$), and Tukey's post hoc test confirmed that the composite significantly outperformed all single-component materials (Figure 6). The enhanced photocatalytic activity was attributed to broader visible-light absorption and more efficient separation and transfer of photogenerated carriers at the heterointerfaces.

Stability and magnetic separation performance analysis

The cycle stability test results and hysteresis loop of the ZnO/Fe_3O_4/CuO nanocomposite material demonstrated that, after five cycles of degradation experiments, the degradation rate of MB by the composite material remained at 90.2 %, decreasing by only 6.6%, and the reaction rate constant did not decrease significantly. The XRD pattern of the composite material after recycling was basically consistent with that of the fresh sample, revealing that its crystal structure was stable with no obvious phase transition or component loss, and it possessed good reusability (Figure 7a). The hysteresis loop showed that the saturation magnetization (M_s) of the composite material was 18.6 emu/g with low remanent magnetization (M_r) and

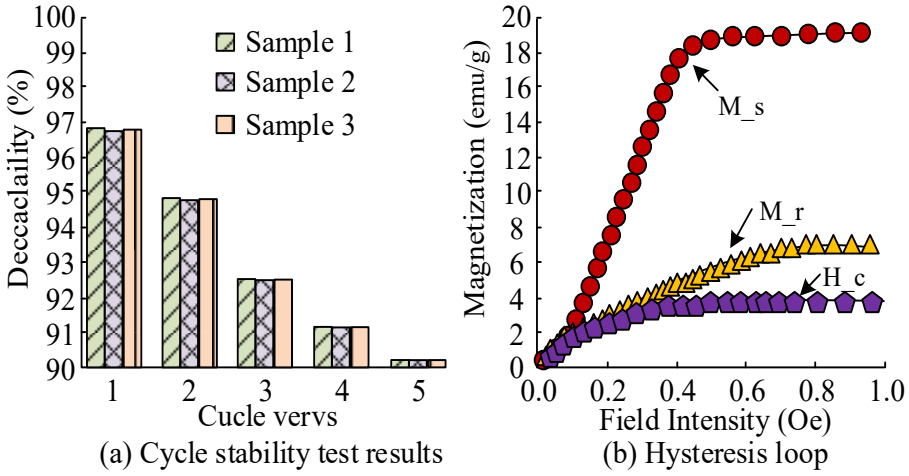

Figure 7. Cyclic stability test results and hysteresis loop of ZnO/Fe_3O_4/CuO nanocomposite.

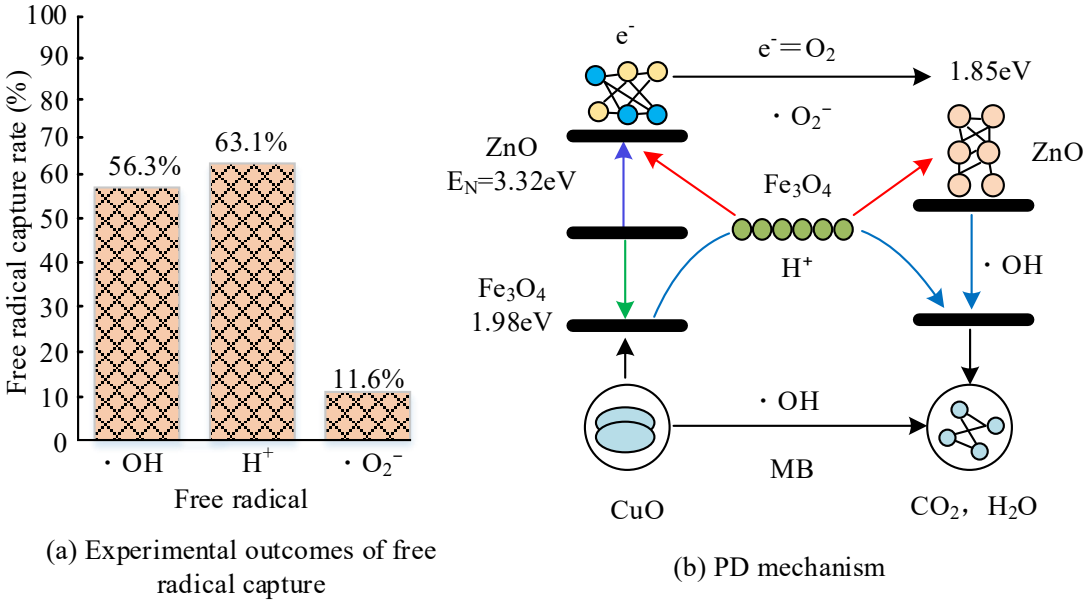

Figure 8. Schematic diagram of free radical capture results and PD mechanism.

coercivity (H_c), exhibiting superparamagnetic characteristics (Figure 7b). The magnetic properties of the composite material enabled its swift separation and recovery using an external magnetic field post-reaction, avoiding secondary pollution and solving the problem of difficult recovery of traditional photocatalysts, which provided convenience for practical wastewater treatment applications. This advantage had important practical value in the research of magnetic separation photocatalytic materials.

Analysis of PD mechanism

The free radical scavenging experimental results and a schematic diagram of the PD mechanism of the ZnO/Fe_3O_4/CuO nanocomposite showed that the degradation rate of MB by the composite material decreased after the addition of IPA (·OH scavenger), EDTA-2Na (H^+ scavenger), and p-BQ ($\cdot O^{2-}$ scavenger), respectively. OH^- and H^+ were the main active species in the PD reaction, contributing approximately 56.3% and 63.1%, respectively, while the contribution of $\cdot O^{2-}$ was

relatively small with approximately 11.6% (Figure 8a). Combining optical properties, electrochemical analysis, and referring to the catalytic mechanisms of related composite materials, the PD mechanism of the ZnO/Fe_3O_4/CuO nanocomposite was proposed (Figure 8b). The band structures of ZnO (E9 = 3.23 eV), Fe_3O_4 (E9 = 1.98 eV), and CuO (E9 = 1.85 eV) were matched, forming a type-II heterojunction. Under VL irradiation, Fe_3O_4 and CuO were excited first, and photogenerated electrons (e-) transition from their valence band (VB) to their conduction band (CB). Since the CB potential of ZnO (-0.31 eV) was more negative than that of Fe_3O_4 (0.28 eV) and CuO (0.08 eV), the e- on the CB of Fe_3O_4 and CuO would transfer to the CB of ZnO. Meanwhile, photogenerated holes (H^+, 2.92 eV) on the VB of ZnO would transfer to the VB of Fe_3O_4 (2.26 eV) and CuO (1.93 eV), forming effective charge separation. The electrons (e-) on ZnO CB reacted with O_2 in the solution to generate O^{2-}, while the hydrogen (H^+) on Fe_3O_4 and CuO VB had strong oxidizing capabilities, directly oxidizing and degrading MB molecules or reacting with H_2O in the solution to generate OH^-. The combined action of OH^- and H^+ decomposed MB molecules into small inorganic molecules such as CO_2 and H_2O, achieving complete degradation of pollutants. The construction of the heterojunction effectively suppressed the recombination of PEH pairs, broadened the photoresponse range, and thus enhanced the VL photocatalytic performance of the composite material.

Conclusion

A ZnO/Fe_3O_4/CuO ternary nanocomposite was successfully prepared using a combined sol-gel-hydrothermal method. The coupling of the three metal oxides formed an effective heterojunction structure, which broadened the visible-light response, promoted photogenerated-carrier separation, and enhanced the photocatalytic degradation of methylene blue. Reactive-species analysis indicated that photogenerated holes and hydroxyl radicals played dominant roles in the degradation process. The composite also exhibited satisfactory structural stability, reusability, and magnetic recoverability. Overall, the integration of photocatalytic activity, cycling stability, and magnetic separation demonstrated the potential of ZnO/Fe_3O_4/CuO nanocomposites for the advanced treatment of dye-containing wastewater and provided a useful strategy for designing multifunctional visible-light photocatalysts.

References

1. Gong C, Lv X, Liu S, Chen X, Weerasooriya R, Ding Z. 2025. Novel α-MnO_2/AC catalysts for heterogeneous catalytic ozonation process to remove BAA in dye wastewater. J Ind Eng Chem. 141(1):340-350.
2. Mahanta R, Chetri P, Shukla N, Tamang SK. 2025. A combined experimental, DFT, and machine learning study of cellulose nanocrystal/SnO_2 composites for efficient sunlight-assisted wastewater remediation. Appl Surf Sci. 712(1):54-59.
3. Laghrib S, Gherdaoui CE, Belgherbi O, Benaskeur N, Boudissa M, Kanagaraj A. 2025. Photocatalytic degradation of methylene blue using TiO_2 nanoparticles synthesized *via* the sol–gel method in acidic and neutral media. React Kinet Mech Catal. 138(3):1725-1745.
4. Shashikala KJ, Kalleshappa CM, Jagadeesh MR, Almalki ASA, Alsanie WF, Alhadharami A. 2026. Polypyrrole-integrated Mg-ZnO nanocomposites: A dual-functional material for photocatalytic RhB degradation and electrochemical sensing. J Appl Polym Sci. 143(2):24-29.
5. Aguinid BJM, Zoleta JB, Alguno AC, Lubguban AA, Asequia DMA, Halun SZB. 2025. Dual-action κ-carrageenan: A novel capping agent and dopant source for enhanced photocatalytic ZnO nanoparticles in azo dye and Cr(VI) degradation. ACS Omega. 10(10):9919-9919.
6. Jaber RH, Ebrahim SE, Omar FM. 2025. Magnetic core/shell Fe_3O_4@FA nanocomposite for visible-light photocatalytic degradation of methyl orange. Int J Des Nat Ecodyn. 20(9):19-35.
7. Hou M, Zhu W, Hao L, Guan S, Lu Y. 2025. Magnetically separable Fe_3O_4/BiOI heterojunction photocatalyst with excellent photocatalytic activity. Appl Phys A. 131(10):35-49.
8. Janene N. 2024. Strong spin-ferromagnetic order and active dye-depollution performance of CuO semiconductor: Gd and Gd/Mn dopants. J Sol-Gel Sci Technol. 109(2):12-14.
9. Valiyathur F, Raza AA, Kottur AB, Sakvai MS. 2024. Synthesis, characterization and photocatalytic activity of alginate-based hybrid material for efficient degradation of organic pollutants under UV light and sunlight irradiation. Carbohydr Polym. 343(1):14-19.
10. Ye J, Beagan AM, Guo SR, Hayat A, Orooji Y. 2025. Synergistic effects in copolymerized carbon nitride/MoO_3 heterojunction

composites for efficient visible-light-driven photocatalysis. EcoMat. 7(5):70015-70023.

11. Liu D, Jiang L, Chen D, Hao Z, Deng B, Sun Y. 2024. Twin S-scheme g-C_3N_4/$CuFe_2O_4$/$ZnIn_2S_4$ heterojunction with a self-supporting three-phase system for photocatalytic CO_2 reduction: Mechanism insight and DFT calculations. ACS Catal. 14(7):18-20.
12. Abdul-Ameer ZN. 2024. ZnO/CuO/CdS heterojunction nanostructures as N-P-N structures for optoelectronic applications. Iraqi J Sci. 65(5):56-66.
13. Lee J, Son N, Shin H, Kim J, Park NK, Kim US. 2024. An eco-efficient dual-function technology: Magnetically recoverable rGO-WO_3/Fe_3O_4 ternary heterojunction catalytic system simultaneously performing malachite green photolysis and Cr(VI) reduction. J Clean Prod. 459(1):16-27.
14. Jiang Z, Lei H, Wu L, Ding Y. 2024. Rapid and low-temperature preparation of zircon ceramic by hydrothermal-assisted sol-gel process and microwave sintering. Ceram Int. 50(1):7-12.
15. Cong VT, Long ND, Huong NT, Thanh VM. 2025. Graphene/Fe_3O_4/CuO nanocomposite for enhanced thermal decomposition of ammonium perchlorate *via* an ultrasonic-assisted method. ACS Omega. 10(31):34331-34341.
16. Nguyen NPT, Nguyen NTT, Nguyen TTT, Nguyen DTC. 2025. Adsorption of methyl red dye onto a novel Fe_3O_4/ZnO/C composite derived from ZIF-8. Arab J Sci Eng. 50(24):20649-20663.
17. Kubheka NSM, Nxumalo EN, Managa M, Moloto MJ. 2025. Enhancing the photocatalytic activity of co-precipitation-synthesized Fe_3O_4/ZnO nanocomposites for rhodamine B degradation. Asian J Chem. 37(3):641-652.